


# Reducing Greenhouse Gas Emission from the Neodymium Oxide Electrolysis. Part I: Analysis of the Anodic Gas Formation

Hanno Vogel<sup>1</sup>  · Benedikt Flerus<sup>1</sup> · Felix Stoffner<sup>1</sup> · Bernd Friedrich<sup>1</sup>

© The Minerals, Metals & Materials Society (TMS) 2016

**Abstract** Neodymium metal is produced nowadays only via Chinese technology, by the electrolysis of neodymium oxide in a  $\text{NdF}_3\text{--LiF}$  electrolyte at about 1050 °C. The process is not automated and is known to emit a large amount of perfluorocarbons (PFCs), with a tremendous greenhouse gas potential. The electrochemical system is analyzed by calculating the theoretical voltages of formation of the relevant anodic gas products. Linear voltammograms are conducted together with a simultaneous off-gas measurement to determine the dynamic behaviors of  $\text{CO}$ ,  $\text{CO}_2$ ,  $\text{CF}_4$ , and  $\text{C}_2\text{F}_6$  in relation to the electrochemical behavior. The measurements show that the PFC emission starts with the occurrence of a partial anode effect, where the first  $\text{CF}_4$  is detected, and the anode is passivated partially. The direct enabling of  $\text{CF}_4$  formation activates the anode again, and at higher voltages, also  $\text{C}_2\text{F}_6$  is formed. The critical current density and voltage of this partial anode effect are determined depending on the oxygen content of the electrolyte to be able to define a process window, with no PFC formation. An estimation of the off-gas emission continuously containing 7 %  $\text{CF}_4$  and 0.7 %  $\text{C}_2\text{F}_6$  leads to an emission of about 20 million t  $\text{CO}_2\text{-eq.}$  per year during the production of 30,000 t/a neodymium, which can explain a part of the gap between the amounts of atmospheric measured PFCs and the data from the aluminum and semiconductor industry. Minimizing the PFC

emission must be the primary goal for the whole rare earth electrolysis.

**Keywords** Rare earth · Neodymium · Electrolysis · Greenhouse gas emission · Off-gas

## Introduction

Neodymium is the most used rare earth metal with a production rate of almost 30,000 t/a [1]. About 30 % of it is employed<sup>1</sup> in permanent magnets [2], leading to more than 1.2 t of neodymium in a modern 7-MW wind-power generator [3]. Nowadays, the world's production of neodymium is achieved completely by Chinese technology in and around China.

The technology of molten electrolysis of neodymium oxide was developed at an industrial scale in China in the 1980s as a circular 3 kA cell having vertical electrodes [4, 5]. In the subsequent decades, its size increased to about 4–6 kA with similar cell design [6]. Only recently, some 10 kA cells were developed, with a rectangular cell wall, but still with the same vertical electrode design [7, 8]. Most published Chinese research works describe the 3 kA cell technology. Because the process characteristics are similar, it is considered as the reference technology [9].

At about 1050 °C, the neodymium oxide as the main raw material is fed into the liquid  $\text{NdF}_3\text{--LiF}$  electrolyte. The neodymium is reduced at the tungsten cathode placed in the cell center where the liquid neodymium drops into a molybdenum crucible from where it is taken out periodically by means of a ladle [10]. At the graphite anode, the complex oxide ions are oxidized, and oxygen reacts with carbon to form the gases  $\text{CO}$  and  $\text{CO}_2$  [11]. At higher

---

The contributing editor for this article was Bart Blanpain.

---

✉ Hanno Vogel  
hanno.vogel@rwth-aachen.de

<sup>1</sup> IME Institute of Process Metallurgy and Metal Recycling, RWTH Aachen University, Intzestraße 3, Aachen, Germany

<sup>1</sup> Percentage in this work is by mass unless otherwise marked.

voltages and current densities, fluorine ions also can be oxidized anodically and form perfluorinated carbons (PFC) like  $\text{CF}_4$  and  $\text{C}_2\text{F}_6$  with a tremendous greenhouse gas potential [12]. The electrochemical conditions of this PFC emission have not been investigated sufficiently, and no data of the industrial process are available. Nevertheless, it is stated that 10 %  $\text{NdF}_3$  is taking part in the anodic reaction leading to a high PFC emission [13, 14].

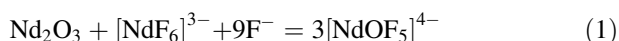
The technological level of the rare earth electrolysis is very low. Usually, only ineffective off-gas suction hoods are often employed, leading to harmful emissions into the environment. However, even with an effective off-gas cleaning equipment in some big factories [15, 16], the produced PFCs are not treated, due to the unavailability of a technical solution [17]. The off-gas treatment facility with a dry adsorption or wet scrubbing system filters HF and fluoride particles, but the gaseous PFCs cannot be filtered. The difference with the aluminum electrolysis is that a majority of the PFC emissions in the aluminum electrolysis happens due to the anode effect, when the cell voltage rises above 8 V [18]. Only recently, it was shown that, also at lower cell voltages, PFCs can be emitted in low concentrations [19]. Still these emissions are quite low in comparison with continuously PFC-producing rare earth electrolysis. Analyzing and understanding the mechanisms of the off-gas evolution in the rare earth electrolysis and determining a basis for an automated process control similar to the comparatively advanced aluminum electrolysis can keep the rare earth electrolysis in a green window of almost PFC-free process.

In part I of this work, the electrochemistry and the anodic gas emission of the neodymium electrolysis are first analyzed, followed by proposing a process control mechanism based on a mathematical cell voltage model, which is experimentally evaluated in part II [20].

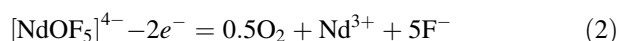
## Electrochemistry of the Electrolytic System and Anodic Gas Evolution

The dissolution of neodymium oxide and the subsequent electrode reactions depend on the complex ions forming in the melt. The most probable reactions are [21]

Dissolution of neodymium oxide :



Anodic reaction :



Cathodic reaction :



The solid oxide particles dissolve in the liquid electrolyte, typically consisting of about 85 %  $\text{NdF}_3$  and 15 %

$\text{LiF}$ , forming  $[\text{NdOF}_5]^{4-}$ . The anodically evolved  $\text{O}_2$  further reacts with carbon to form gaseous  $\text{CO}$  and  $\text{CO}_2$ , while the free  $\text{Nd}^{3+}$  and  $\text{F}^-$ -ions form complex ions, probably of  $[\text{NdF}_6]^{3-}$  [22]. This ion typically reacts cathodically and forms liquid neodymium and  $6\text{F}^-$  as shown in Fig. 1.

The overall reaction is independent of the individual complex ion and intermediate reaction steps. The most probable overall reactions are listed in Table 1 [23]. The decomposition reactions of  $\text{LiF}$  are not included, because of the high theoretical voltages making it unlikely to happen. The formation of  $\text{CO}$  at 1.3 V is thermodynamically the first enabled reaction, followed by  $\text{CO}_2$  at just about 0.16 V higher. Looking at the thermoneutral voltage, the formation of  $\text{CO}_2$  reaches the thermodynamic equilibrium at the voltage of 2.11 V, while during a  $\text{CO}$ -producing electrolysis needs a voltage of 2.55 V to maintain the heat balance of the reaction.

The cooxidation of oxide and fluoride is enabled at only 0.5 V higher than that required for the  $\text{CO}_2$  formation. During the reaction with carbon, the unstable  $\text{COF}_2$  and  $\text{COF}$  molecules are formed, which probably reacts further with carbon to produce  $\text{CF}_4$  and  $\text{CO}$ . At 2.75 V and at 2.98 V, the direct formation of  $\text{CF}_4$  and that of  $\text{C}_2\text{F}_6$  are enabled, respectively. The voltage differences between oxide and fluoride oxidation are not high. Because the voltage of formation of the specific anode product is not only dependent on the temperature but also on the current density and especially on the concentration of the dissolved reacting species in the electrolyte at the interface with the anode, the process can change easily from oxide to fluoride oxidation.

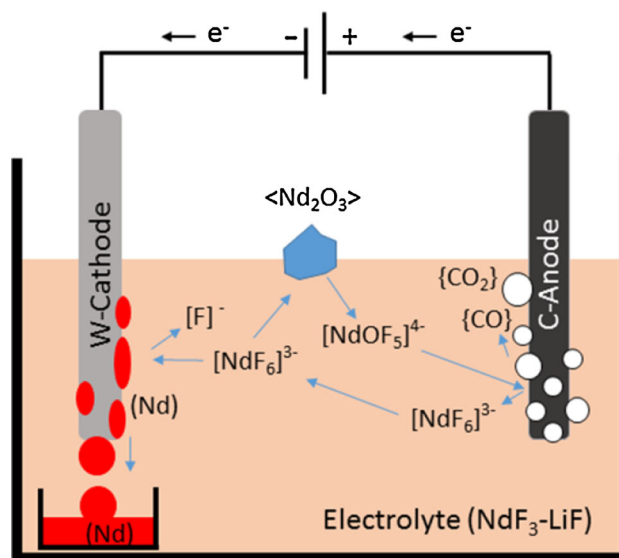


**Fig. 1** Principal dissolution and reaction mechanisms of the neodymium oxide electrolysis

With rising voltage, the current density of the system increases until it reaches the critical current density when another reaction is enabled. Depending on the product, a passivation of the anode can happen, leading to a breakdown of the electrolysis, called anode effect, as a well-known occurrence during the aluminum electrolysis [24]. As for the neodymium electrolysis, there have been no investigations published so far about the gaseous emission from industrial cells in relation to the anodic voltage and current density. Only results from laboratory research can give insight into the components and amounts of the anodic reaction. A Chinese laboratory investigation of the electrolysis gas shows increasing levels of CO with the increasing temperature and increasing CO<sub>2</sub> levels with the increasing current density. At 1050 °C with a current density of 1.0 A/cm<sup>2</sup>, a CO/CO<sub>2</sub>-ratio of 3.1 was found [11] but no PFC compounds are documented. Another study analyzes gas samples in relation to the electrolysis cell voltage and finds, at about 6 V, C<sub>2</sub>F<sub>6</sub> as the predominant gas component with about 70 % [12]. To evaluate the anodic gas evolution, the precise oxide concentration and current density need to be measured.

## Experimental Setup

The electrolyte is prepared from pure NdF<sub>3</sub> with 99.9 % (Treibacher Industrie AG) and LiF with 99.85 % (Alfa Aesar GmbH & Co KG) purity. The powder with 85 % NdF<sub>3</sub> and 15 % LiF is dried overnight at 300 °C and then melted in a sealed furnace with 1.4 bar argon 5.0 atmosphere. The fluoride mixture is homogenized in a pure graphite crucible by superheating it shortly and then poured into a thin graphite mold for rapid solidification. The solid electrolyte is broken into pieces, and about 500 g is put in a pure graphite crucible (SIGRAFINE® R8510; SGL Carbon) of 6.5-cm inner diameter and 8-cm height. Nd<sub>2</sub>O<sub>3</sub> powder with 99.9 % purity (Alfa Aesar GmbH & Co KG) is dried at 300 °C overnight and used as feeding-stock material. The graphite crucible is placed in a sealed steel container with a water-cooled lid, continuously flushed with pure argon 5.0 at flow rate of 3 l/min. The steel cell is placed in a resistance-heated furnace. Through the lid, a Pt-PtRh-thermocouple with molybdenum sheath of 4-mm diameter (Omega Engineering GmbH) is dipped in the liquid electrolyte set to a temperature of 1050 °C with a deviation of about 10 K due to electrolysis heat generation. From top, the rod-like anode and cathode are placed in the electrolyte with about 2–3-cm immersion depth. The pure graphite (SIGRAFINE® R8510; SGL Carbon) anode has a diameter of 6 mm and the pure tungsten cathode (99.95 %; PLM GmbH) a diameter of 4 mm. As reference electrode, a graphite rod, a 1-mm-diameter tungsten or platinum wire

is employed. The linear and two-way voltammograms are measured by a potentiostat (IviumStat; Ivium Technologies) with a capacity of 5 A at 8 V. The anodic cell resistance is calculated by the linear increase in current in relation to the voltage between the anode and the reference electrode up to the occurrence of first passivation phenomenon. The off-gas is analyzed continuously by taking 1 l/min from the cell atmosphere and pumping it at 180 °C through the FT-IR-spectrometer (Gasmeter, Ansyco), which is calibrated for all relevant gases. The measuring time interval is 7 s, to allow for the superimposition of the dynamic off-gas and current behaviors over the voltage. Electrolyte samples are drawn out using argon-filled pure glass pipettes (HSQ300; Quarzglas Heinrich) with an inner diameter of 2.5 mm to determine the oxygen content. The pipette is dipped to a depth of 2 cm in the electrolyte close to the anode, where the sample of about 1 g is taken out of the cell to be analyzed by the carrier gas method.

## Results and Discussion

The current density behavior in relation to the voltage is shown in the linear voltammogram of Fig. 2. Beyond the decomposition voltage, the current density increases exponentially, until it reaches the first peak, where a semi-passivation happens and the current density drops to about the half value. Afterward, the current increases at a slower rate than before terminating at the total passivation voltage stage, above which no significant current flows, as has already been shown [13]. Always two peaks can be observed. The first peak can be termed the *partial anode effect* and the second one *full anode effect*. Their exact values of voltage and current density vary significantly with the addition of neodymium oxide. The anodic passivation phenomenon at the partial anode effect is strongly

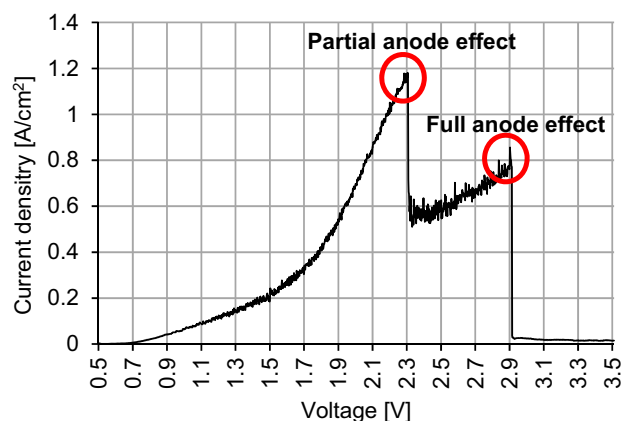


**Fig. 2** Linear voltammetry with partial and full anode effect versus tungsten with 10 mV/s at 1050 °C in 85 NdF<sub>3</sub>–15 LiF and addition of 0.5 % Nd<sub>2</sub>O<sub>3</sub>

influenced by the oxygen concentration, whereas the full anode effect is less influenced by the amount of oxide added, as shown below. The linear voltammetry is shown in Fig. 2, where 0.5 %  $\text{Nd}_2\text{O}_3$  is added to the  $\text{NdF}_3\text{--LiF}$  electrolyte. The partial anode effect reaches a higher current density than that of the full anode effect.

The two-way linear voltammetry of the anodic potential up to 8 V is shown in Fig. 3. Here no extra oxide is added, but the oxygen analysis shows a content of about 2000 ppm, which equals 1.4 %  $\text{Nd}_2\text{O}_3$ . There are again two peaks detectable, while at the lower oxide concentration the partial anode effect is reached at 0.4  $\text{A}/\text{cm}^2$  but the full anode effect happens at the similar current density like in Fig. 2 of about 0.8  $\text{A}/\text{cm}^2$ . With higher scanning velocity, the full anode effect reaches a higher voltage and current. On the reverse scan coming from the passivated state the slope of increasing current is independent of the velocity between 25 and 200  $\text{mV}/\text{s}$ . All curves increase at the same

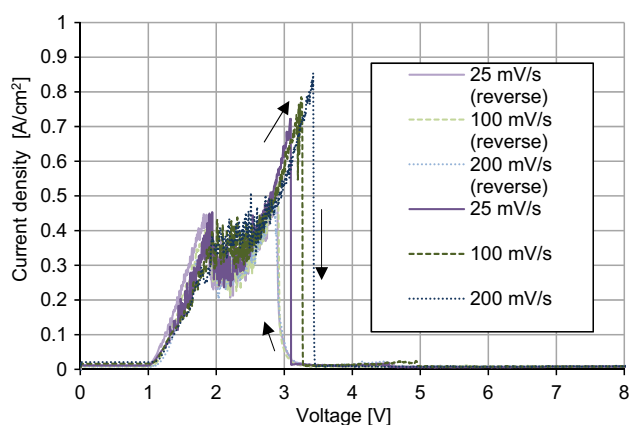


**Fig. 3** Two-way linear voltammetry within the range of 0–9.9–0 V with variation of scanning velocity versus graphite at 1050 °C in 85  $\text{NdF}_3\text{--}15 \text{ LiF}$  without addition of  $\text{Nd}_2\text{O}_3$

rate, starting at the same voltage. This means the anode passivation is reversible and directly dependent on the voltage, which is here 3.3 V against graphite.

Analysis of the off-gas evolution while conducting the linear voltammetry CO appears to reveal the predominant gas component, as shown in Fig. 4. The background CO concentration of about 170 ppm is due to oxygen impurities in the cell atmosphere forming CO while reacting with carbon of the graphite anode and crucible. The oxygen impurity can originate from the argon gas flushing and also from humidity in the premelted electrolyte and the cell setup material. Neglecting the base concentration, CO is the first gas component to evolve as the current increases at 1.1 V versus graphite.  $\text{CO}_2$  is detected immediately after the CO emission, starting at about 1.4 V. For better visibility, the  $\text{CF}_4$  concentration is plotted with a factor of 100, meaning the peak value is about 150 vol-ppm. The  $\text{CF}_4$  formation starts at about 2.8 V.  $\text{C}_2\text{F}_6$  is found only in traces with about 2 vol-ppm starting at about 0.5 V higher voltage compared with the  $\text{CF}_4$  formation, which is not depicted in Fig. 4. This measured voltage differences of the start of CO,  $\text{CO}_2$ ,  $\text{CF}_4$ , and  $\text{C}_2\text{F}_6$  formation are in good accordance with the calculated thermodynamic values given in Table 1. The voltage deviations can be attributed to small errors in the time synchronization of the voltammetry and the off-gas measurement. The Boudouard reaction can decrease the  $\text{CO}_2$  and increase the CO content slightly because the gas phase has time to react with the free graphite of the anode and crucible before being pumped into the analyzer tube. At 1050 °C, the theoretical Boudouard equilibrium is completely on the CO side [25].

The effect of the partial anode effect is clearly visible in the gas composition. The rise in  $\text{CO}_2$  concentration stag-nates in the semipassivated state, while the CO evolution is only slightly influenced by the partial anode effect, while

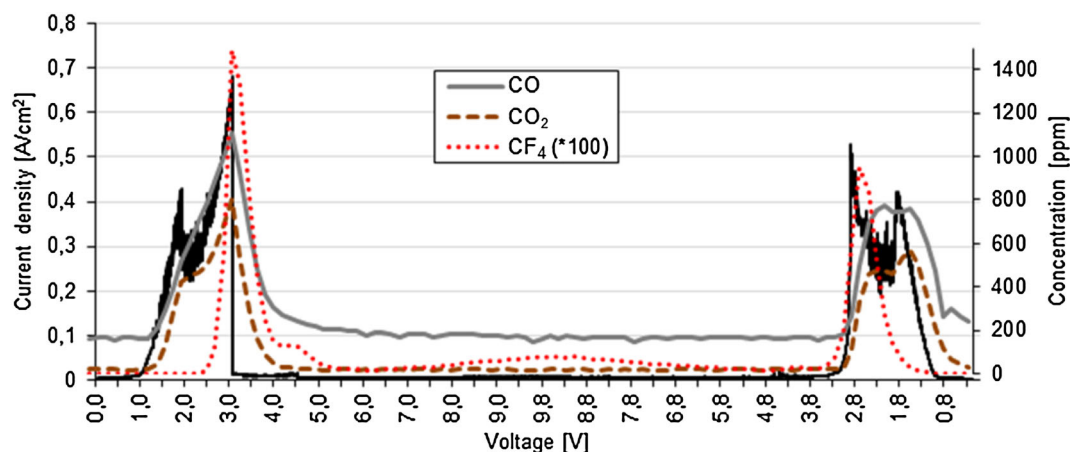


**Fig. 4** Continuous off-gas measurement in vol-ppm at two-way linear voltammetry (0–10–0 V) with 25  $\text{mV}/\text{s}$  versus graphite at 1050 °C in 85  $\text{NdF}_3\text{--}15 \text{ LiF}$  without additional  $\text{Nd}_2\text{O}_3$

**Table 1** Theoretical decomposition enthalpies and corresponding voltages of common reactions with highlighted gaseous products at 1050 °C as determined by FactSage<sup>TM</sup> 6.4

No.	Reaction	Gibbs free energy, $\Delta G$ (J/mol)	Enthalpy, $\Delta H$ (J/mol)	Electron transfer, $n$	theoretical decomposition voltage, $E_G^0$ (V)	Thermoneutral voltage, $E_H^0$ (V)
1	$\text{Nd}_2\text{O}_3 + 3\text{C} \rightarrow 2\text{Nd} + 3\text{CO}$	750,893	1,473,194	6	1.297	2.545
2	$\text{Nd}_2\text{O}_3 + 3/2\text{C} \rightarrow 2\text{Nd} + 3/2\text{CO}_2$	841,707	1,222,320	6	1.454	2.111
3	$\text{H}_2\text{O} + 2/3\text{NdF}_3 + \text{C} \rightarrow 2/3\text{Nd} + \text{CO} + 2\text{HF}$	284,174	691,082	2	1.472	3.581
4	$\text{Nd}_2\text{O}_3 + 2\text{NdF}_3 + 3\text{C} \rightarrow 4\text{Nd} + 3\text{COF}_2$	2,429,722	3,210,509	12	2.099	2.773
5	$\text{Nd}_2\text{O}_3 + \text{NdF}_3 + 3\text{C} \rightarrow 3\text{Nd} + 3\text{COF}$	2,119,937	2,949,363	9	2.441	3.396
6	$\text{NdF}_3 + 3/4\text{C} \rightarrow \text{Nd} + 3/4\text{CF}_4$	796,459	960,670	3	2.752	3.319
7	$\text{NdF}_3 + 3/4\text{C} \rightarrow \text{Nd} + 3/4\text{C}_2\text{F}_6$	861,163	993,074	3	2.975	3.431
8	$\text{NdF}_3 + 3/2\text{C} \rightarrow \text{Nd} + 3/2\text{CF}_2$	1,012,197	1,381,578	3	3.497	4.773
9	$\text{NdF}_3 + 3\text{C} \rightarrow \text{Nd} + 3\text{CF}$	1,689,202	2,418,927	3	5.836	8.357

Data Fact PS, FT salt

$\text{CF}_4$  is first detected. The thermodynamic values suggest a cooxidation of oxide and fluoride forming  $\text{COF}_2$ , which is unstable and probably reacts with carbon to form  $\text{CF}_4$  and  $\text{CO}$ . When the direct  $\text{CF}_4$  formation is enabled at a 0.65 V higher voltage compared with the enabling of  $\text{COF}_2$  formation, the current can again rise very fast. All gas components reach their maximum values at the full anode effect where  $\text{CF}_4$  evolution reaches to 150 vol-ppm, which equals 8 % of the total  $\text{CO}$  and  $\text{CO}_2$  contents. After the full anode effect, all gas components return to almost zero. Only  $\text{CF}_4$  rises slowly with the increasing voltage to a maximum of 7 vol-ppm at 9.9 V. The partial anode effect can be regarded as the starting point of  $\text{CF}_4$  evolution and for the general start of PFC emissions. Other PFCs and fluoride compounds like  $\text{COF}_2$ ,  $\text{OF}_2$ , and  $\text{C}_5\text{F}_8$  were measured continuously, but could not be detected with assured reliability in the anodic gas. Due to dilution caused by the flushing gas, some small quantities of these compounds might still be formed.

The reverse scan from 10 to 0 V with regard to the corresponding gas evolution shows a similar behavior. The  $\text{CF}_4$  concentration coming from 10 V decreases again only with a small bump at 4.2 V and increases as the first gas component followed by  $\text{CO}_2$  and  $\text{CO}$ . The almost full passivation vanishes with a strong  $\text{CF}_4$  emission, leading to the conclusion that the full passivation phenomenon is a reversible anode reaction with  $\text{CF}_4$  as a product, while the reactivation happens. The voltage of the full anode effect can enable the formation of a solid C–F layer with intercalated fluorine [26]. This dielectric layer can be formed by a 1.7-nm-thin CF and  $\text{CF}_2$  inhomogeneous structure [27]. The change in surface energy by this growing layer results in a gas-shield cover on top of this layer, creating total electrical insulation of the anode.

In Fig. 5, the voltage and current density behavior are plotted for 0.5 % stepwise increase of oxide additions up to 2.5 % with a slow scanning speed of 5 mV/s, showing a good current–emission correlation. The individual gas components are influenced by the oxide concentrations. In Fig. 6, the corresponding concentration ratios of  $\text{CO}$  to  $\text{CO}_2$  are shown with the voltages of the partial and full anode effects. The uneven curve reaches its minimum before the partial anode effect, from where the  $\text{CO}/\text{CO}_2$  ratio increases fast. Between the partial and full anode effects, the  $\text{CO}/\text{CO}_2$  ratio reaches its maximum, only slowly decreasing before proceeding into the full anode effect. Another tendency becomes obvious. The higher the oxide content of the electrolyte becomes, the higher is the  $\text{CO}$  content compared with  $\text{CO}_2$  in the anodic gas. In Fig. 7, the  $\text{CF}_4$  emission is plotted in relation to the voltage. The maximum  $\text{CF}_4$  value at 0 % oxide addition reaches 10 ppm and is more than 10 times higher than the detected maximum value after the addition of 0.5 %  $\text{Nd}_2\text{O}_3$ . The formation of  $\text{CF}_4$  is clearly shifted to higher voltages with the increasing oxide content of the electrolyte, because with the higher critical current density of the partial anode effect, more oxide is dissolved in the electrolyte.

The precise mode of current density and gas evolution is dependent on the electrolyte composition. The concentration of the oxygen-containing complex ions at the anode surface has the strongest influence. Because of the little solubility of neodymium oxide in the electrolyte, the formation of a sludge at the cell bottom is likely to happen while feeding oxide in the liquid electrolyte. Hence, there is always a discrepancy between the amount added and the true oxygen concentration near the anode surface. From the plots of the current density–voltage curves at a wider range



**Fig. 5** Linear voltammograms for increasing oxide feeding amounts at 5 mV/s versus tungsten at 1050 °C in 85 NdF<sub>3</sub>-15 LiF

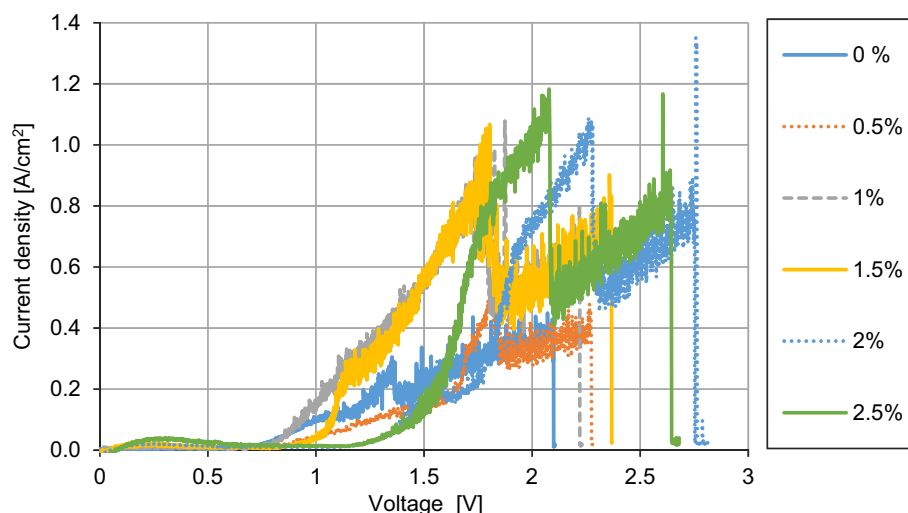


**Fig. 6** Concentration ratio CO/CO<sub>2</sub> of the linear voltammetry (Fig. 5) at different neodymium oxide feeding amounts with square marks showing the partial anode effect and round marks showing the full anode effect

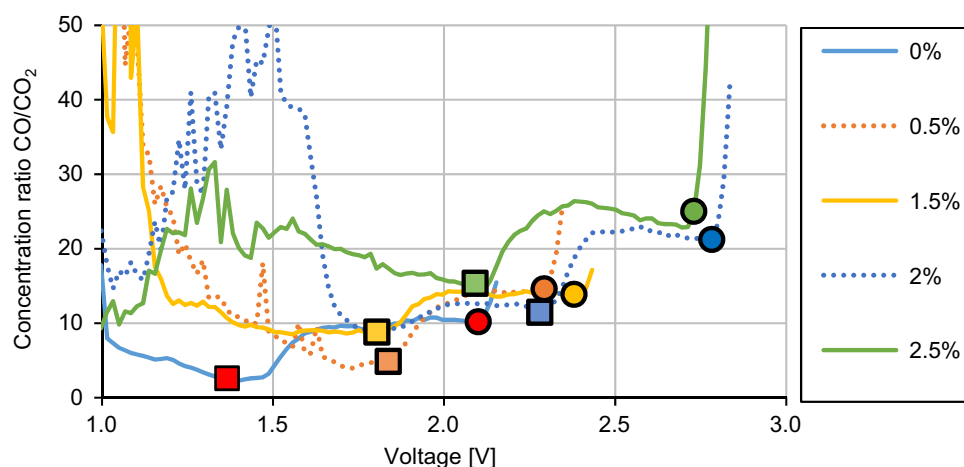
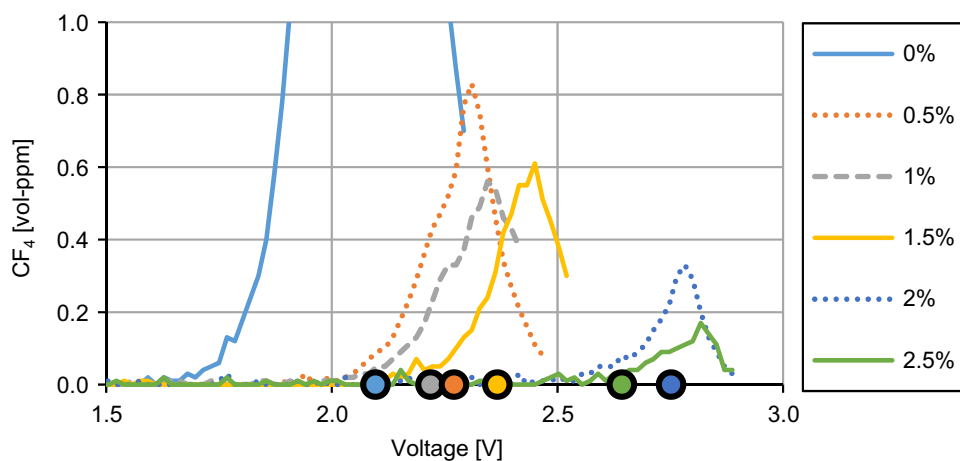


**Fig. 7** CF<sub>4</sub> formation over voltage of the linear voltammetry (Fig. 5), with values of the full anode effect as round marks; maximum value of 0 % at 10 ppm



of neodymium oxide amounts together as shown in Fig. 8, the former observations becomes clear. The more amount of oxide is fed, the higher becomes the critical current density and voltage of the partial anode effect, as seen from the circles in Fig. 8. The amount of fed neodymium oxide

in 0.5 % steps is given on top in the legend, starting from 0 % up to a sum of 4 %. In brackets, the actual measured oxygen concentrations calculated as Nd<sub>2</sub>O<sub>3</sub> are given as well, showing an extreme deviation in the theoretical and actual oxide contents of the electrolyte. The difference in

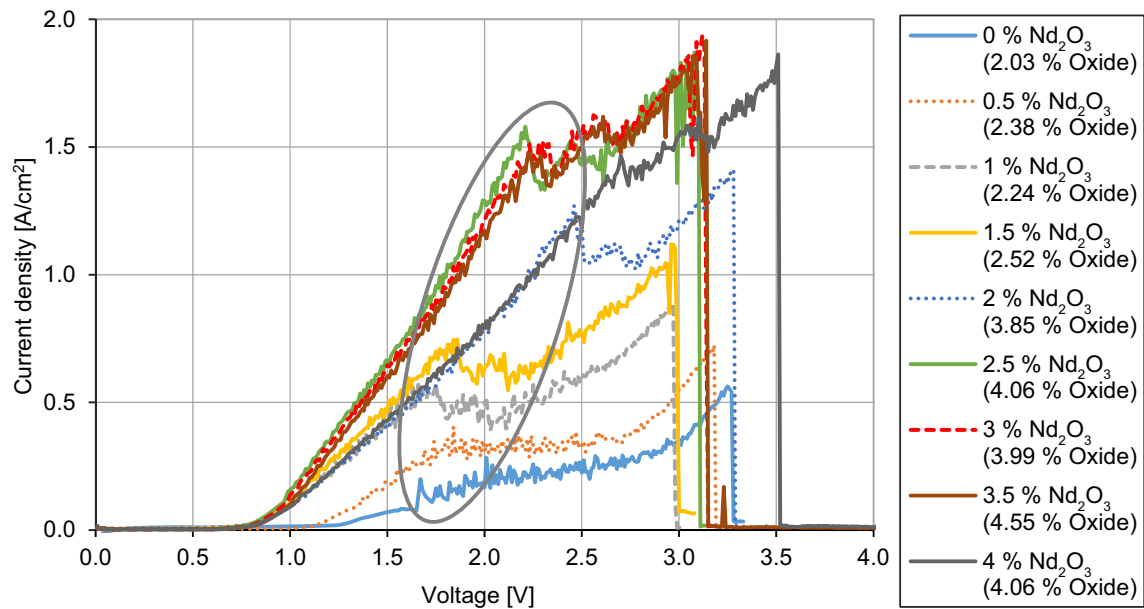


**Fig. 8** Linear voltammograms for increasing oxide feeding amounts at 50 mV versus Pt-wire at 1050 °C in 85 % NdF<sub>3</sub>–15 % LiF (510.5 g)

the curves due to the rising oxygen concentration at the anode is mainly due to the anodic overvoltage and the concentration-dependent decomposition voltage. The strongest influence on the anodic overvoltage according to Vogt [28] can be given as:

$$\eta = \frac{RT}{\alpha F} \left[ \ln \frac{I}{A(1-\theta)j_0} - \ln \left( \frac{v_A}{v_e} \frac{1}{Fk_A c_\infty} \right) \right], \quad (4)$$

where  $\eta$  = overvoltage,  $\alpha$  = charge transfer factor,  $F$  = Faraday constant,  $R$  = ideal gas constant,  $T$  = temperature,  $I$  = current,  $A$  = anode surface,  $\theta$  = coverage of anode surface by bubbles,  $j_0$  = exchange current density (about 100 mA/cm<sup>2</sup>);  $k_A$  = mass transfer coefficient,  $c_\infty$  = concentration of reacting species in electrolyte, and  $\frac{v_A}{v_e}$  = stoichiometric number of reacting species per number of electrons.

The active anode area is reduced by its bubble coverage, expressed in the left term. The right term describes the resistance due to charge transfer, where  $c_\infty$ —the bulk concentration of Nd<sub>2</sub>O<sub>3</sub>—is the changing parameter, resulting in high overvoltage when the concentration approaches zero. This overvoltage is the main parameter for determining the oxygen concentration by voltage, which is necessary for a process control, similar to the aluminum electrolysis, as described in part II of this work [20]. This overvoltage in relation to the current can be expressed as the cell resistance. Fig. 9 shows the anodic half-cell resistance in relation to the oxide feeding amount. A significant increase in resistance is evident with respect to an amount of 2.5 % neodymium oxide. Because of the difficulty in dissolving the oxide, the true oxide concentration varies as

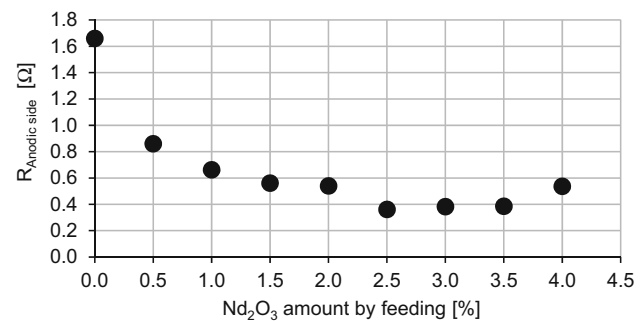


**Fig. 9** Resistance of the anodic side of the electrolysis cell calculated by the linear increase of the current versus the voltage up to the partial anode effect over the feeding amount of oxide

described above. By plotting the same resistance values in relation to the measured oxygen concentrations, which are calculated with respect to the Nd<sub>2</sub>O<sub>3</sub> amounts in Fig. 10, we find that this tendency is shifted to a higher oxide concentration, meaning that the resistance can become much higher for even lower oxide contents. It is therefore necessary to run a cleaning electrolysis step to lower the starting amount of oxygen in the system. Still, the general relation of oxide content and cell resistance is proven and can be taken as the basis for a process control strategy, which is elaborated in part II [20].

The current density and voltage of the partial anode effect should not be surpassed to avoid the emission of PFCs. From the plots of the points of the partial anode effects against the oxide concentrations added to the electrolyte of the two measurements in Figs. 5 and 8, a deviation with the increasing scanning velocity is found, as shown in Fig. 11.

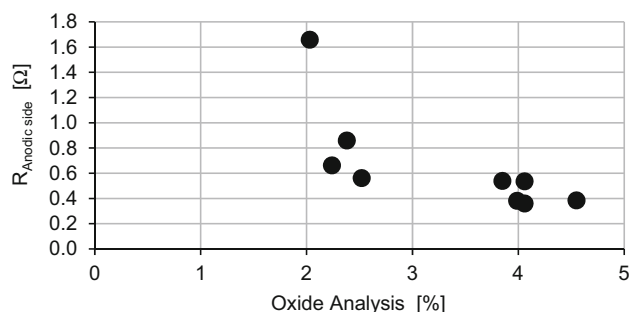


**Fig. 10** Resistance of the anodic side versus the real measured oxygen value given as the neodymium oxide percentage

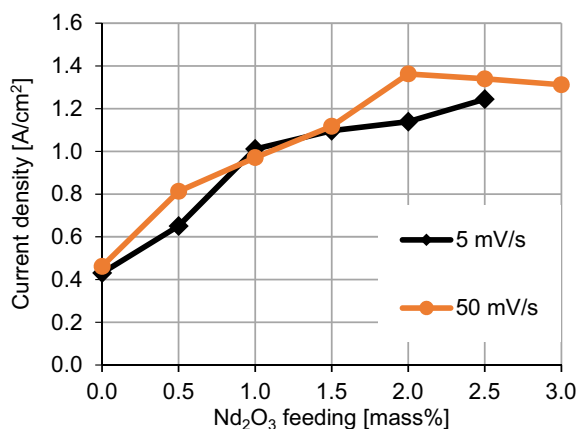


**Fig. 11** Dependence of the critical anode current density at the partial anode effect on the addition of neodymium oxide at 5 and 50 mV/s scanning velocity

The galvanostatic electrolysis needs to stay below this critical current density to guarantee a PFC-free neodymium production. By conducting a continuous neodymium electrolysis maintained at an anodic current density of, e.g., 1 A/cm<sup>2</sup> with an oxide concentration of 2.5 %, the process proceeds on the basis of a sustainable CO–CO<sub>2</sub> emission. If the oxide feeding is not sufficient, the oxide concentration decreases to, e.g., 0.5 %, and the critical current density is surpassed leading to CF<sub>4</sub>–C<sub>2</sub>F<sub>6</sub> emission.

According to an emission measurement of a galvanostatic electrolysis with a mass of 2 kg of electrolyte and a ring-shaped anode similar to the industrial cell setup, the off-gas can contain continuously about 10 vol-ppm CF<sub>4</sub> and 1 vol-ppm C<sub>2</sub>F<sub>6</sub>, leading to a severe sustainability issue in terms of emission [20].

A continuous anodic gas composition of 7 % CF<sub>4</sub> and 0.7 % C<sub>2</sub>F<sub>6</sub> with 80 % current efficiency would yield a CF<sub>4</sub> mass of 0.0739 kg and a C<sub>2</sub>F<sub>6</sub> mass of 0.0116 kg per kilogram neodymium produced. With the numbers of CO<sub>2</sub>-equivalents of CF<sub>4</sub> being 7390 and of C<sub>2</sub>F<sub>6</sub> being 12,200 [29], a sum of about 700 kg CO<sub>2</sub>-eq./kg<sub>Nd</sub> is obtained. This

is an enormous amount, compared to about 2 kg CO<sub>2</sub>-eq. per kg aluminum [30]. The neodymium production adds up to almost 30,000 t per year [1]. Summing this hypothetical neodymium electrolysis emission values up for 1 year, the total amount accumulates to more than 20 million t CO<sub>2</sub>-eq. that is a climate-relevant amount and an unneglectable issue. Atmospheric PFCs are attributed so far only to the aluminum electrolysis and semiconductor industry not taking into account the probable heavy contributions to the atmosphere by the rare earth electrolysis [31]. The gap between industry data and atmospheric measurements is about 4 kt in 2010. This equals, assuming a C<sub>2</sub>F<sub>6</sub>/CF<sub>4</sub> mass ratio of 0.1, about 30 million t CO<sub>2</sub>-eq. The gap from the year 2000 on could be explained partly by the increasing amount of rare earth electrolysis. If the neodymium electrolysis emits only CO or CO<sub>2</sub>, a greenhouse potential of less than 0.5 kg CO<sub>2</sub>-eq. per kilogram of neodymium can be achieved, with the cumulative sum of the total year production of being less than 15,000 t CO<sub>2</sub>-eq.

Not only neodymium but also praseodymium and misch metal are produced the same way. Even some heavy rare earth metals are electrolyzed by using a consumable iron cathode to produce for example Dy–Fe. Hence, the sum of rare earth metals produced by rare earth electrolysis exceeds the estimated production of neodymium by 30,000 t in 2016 and makes the sustainability issue even more serious. Minimization of the PFC emission needs to be the primary goal of the rare earth electrolysis. An approach is proposed in part II [20].

## Conclusion

The behavior of the electrochemical system at linear voltammetries of NdF<sub>3</sub>–LiF–Nd<sub>2</sub>O<sub>3</sub> shows a first passivation, termed the partial anode effect, where the current density falls turbulent with the increasing voltage. Here the most probable reaction is the oxidation of oxide and fluoride ions reacting with carbon to COF and COF<sub>2</sub>, which probably reacts further at the carbon anode to form CF<sub>4</sub> and CO. This electrochemical effect marks the beginning of the PFC emission, followed by CF<sub>4</sub> and then by C<sub>2</sub>F<sub>6</sub>. At a higher voltage, the full anode effect is reached with an almost full passivation of the anode. This passivation is reversible and probably due to the formation of a C–F-layer, which is covered by a gas-shield layer, thereby electrically insulating the anode completely.

The oxide feeding does not lead to an equal amount of dissolved oxide in the electrolyte, making the feeding procedure important with the need to control carefully to avoid a sludging of the cell bottom. The critical current density, and consequently the amount and voltage of PFC



emission, is highly dependent on the oxide concentration and ranges from 0.4 to about 1.4 A/cm<sup>2</sup>. In the absence of automation in the process control of the neodymium electrolysis, the surpassing of the partial anode effect is likely to happen. Because the vertical anode does not run directly into full anode effect when PFCs are formed, the process can be conducted continuously above the partial anode effect with PFC emission. Without an automated oxide feeding system based on the cell voltage, this is very likely to happen. With an assumed off-gas content of 7 % CF<sub>4</sub> and 0.7 % C<sub>2</sub>F<sub>6</sub> the neodymium production of 30,000 t/a results in a greenhouse gas emission of about 20 million t of CO<sub>2</sub>-equivalents.

## References

- Kingsnorth D (2015) The global rare earth industry today—plagued by illegal production in China. In: 11th International Rare Earth Conference, Metal Events Ltd's, Singapore
- Gupta CK, Krishnamurthy N (2005) Extractive metallurgy of rare earths. CRC Press, Boca Raton, FL
- Metal Events Ltd. (2014) Report of Metal Events Ltd's 10th International Rare Earths Conference, 11–13 November 2014, Singapore
- Fu S (2007) Present condition of research and developing trend in the rare earth electrolysis cell. *J Chin Rare Earth Soc* 25:71–76 (**Translated from Chinese**)
- Zhang Z (1995) The development of preparing RE metal by oxide electrolysis and the current situation in China. *Non-ferr Metal Smelt* 4:32–35 (**Translated from Chinese**)
- Zhang Z et al (2001) Present situation and latest progress of process for producing metallic neodymium by electrolysis of neodymium oxide with fluoride salts. *Non-ferr Smelt* 30(2):23–25 (**Translated from Chinese**)
- Wang J, Deng ZM, Zhang XL (2004) The test research on energy balance of 10 kA fluoride system in RE fused-salt electrolysis cell. *Jiangxi Nonferr Metals* 18(2):30–33 (**Translated from Chinese**)
- Wen H et al (2004) Circular 10 kA molten salt electrolyzer for preparing rare earth metal. Ganzhou Keli Rare Earth New Materials Co., Ltd (CN 02240881.9) (**Translated from Chinese**)
- Vogel H, Friedrich B (2015) Development and research trends of the neodymium electrolysis—a literature review. In: GDMB (ed) Proceedings of the 8th European metallurgical conference (EMC) 2015
- Pang S et al (2011) Development on molten salt electrolytic methods and technology for preparing rare earth metals and alloys in China. *Chin J Rare Metals* 35(3):440–450 (**Translated from Chinese**)
- Liu K-R et al (2001) Analysis of anodic gases in neodymium electrolysis. *Chin J Nonferr Metals* 11(6):1118–1121 (**Translated from Chinese**)
- Keller R, Larimer KT (1997) Anode effect in neodymium oxide electrolysis. *Rare Earths Sci Technol Appl III(IX)*:175–180
- Li B, Liu S, Wang H, Zhao Z (2014) Electrochemistry for Nd electrowinning from fluoride-oxide molten salts. In: Neelameggham, NR et al (ed) *Rare Metal Technology* 2014 TMS, Warrendale, PA; Wiley, Hoboken, NJ, pp 95–98
- Zhang X, Deng Z, Wang J, You H (2003) Continuous electrolysis of RE metals with block-like multi-anodes. *Jiangxi Nonferr Metals* 17(3):28–30 (**Translated from Chinese**)
- Cheng YD, Liang Y, Tao D (2011) Clean production technology in electrolysis process in a rare earth plant. *Chin Rare Earths* 32(5):92–96 (**Translated from Chinese**)
- Ou YH, Zhou CS (2006) Study on the recovery and utilization of smoke dust in rare earth electrolysis. *Jiangxi Nonferr Metals* 20(1):33–36 (**Translated from Chinese**)
- Chase R et al (2005) PFC emissions performance for the global primary aluminum industry. In: Kvande, H (ed) *Light Metals* 2005, pp 279–282
- Marks J (1998) PFC emission measurements from ALCOA aluminum smelters. In: Welch BJ (ed) *Light Metals* 1998, TMS, Warrendale, PA, pp 287–291
- Thonstad J, Sverre R, Keller R (2013) On the mechanism behind low voltage PFC emissions. In: Sadler B (ed) *Light Metals* 2013. TMS, Warrendale, PA; Wiley, New York, pp. 883–885
- Vogel H, Friedrich B (2016) Reducing greenhouse gas emission from the neodymium oxide electrolysis: Part II. Basics of a process control avoiding PFC emissions. *J Sustain Metall* (unpublished article)
- Stefanidaki E, Hasiotis C, Kontoyannis C (2001) Electrodeposition of neodymium from LiF–NdF<sub>3</sub>–Nd<sub>2</sub>O<sub>3</sub> melts. *Electrochim Acta* 46(17):2665–2670. doi:10.1016/S0013-4686(01)00489-3
- Stefanidaki E, Photiadis GM, Kontoyannis CG et al (2002) Oxide solubility and Raman spectra of NdF<sub>3</sub>–LiF–KF–MgF<sub>2</sub>–Nd<sub>2</sub>O<sub>3</sub> melts. *J Chem Soc Dalton Trans* 11:2302–2307. doi:10.1039/b111563b
- Liu KR et al (2001) Theoretical decomposition voltage for some related substance on neodymium electrolysis. *Chin Rare Earths* 22(2):30–33 (**Translated from Chinese**)
- Thonstad J, Utigard TA, Vogt H (2000) On the anode effect in aluminum electrolysis. In: Peterson RD (ed) *Light Metals* 2000, TMS, Warrendale, PA, pp 131–138
- Neumüller O (1979) *Römpss Chemie-Lexikon*. Franckh'sche Verlagshandlung, Stuttgart
- Groult H et al (2007) Characteristics of the fluorocarbon surface film generated on carbon anode during F<sub>2</sub> evolution in molten KF–2HF. *J Electrochem Soc* 154(6):331–338
- Bai L, Conway BE (1990) Electrochemistry of anodic fluorine gas evolution at carbon electrodes: Part II. Studies on the 'CF' film by the current-interruption, AC impedance, ESCA and auger techniques. *J Appl Electrochem* 20(6):916–924. doi:10.1007/BF01019566
- Vogt H (2013) On the various types of uncontrolled potential increase in electrochemical reactors—the anode effect. *Electrochim Acta* 87:611–618. doi:10.1016/j.electacta.2012.09.051
- Hall C (2009) Key greenhouse gases and global warming potentials. [http://www.ipcc.ch/publications\\_and\\_data/publications\\_ipcc\\_fourth\\_assessment\\_report\\_wg1\\_report\\_the\\_physical\\_science\\_basis.htm](http://www.ipcc.ch/publications_and_data/publications_ipcc_fourth_assessment_report_wg1_report_the_physical_science_basis.htm). Accessed 24 Feb 2016
- Iffert M, Opgen-Rhein J, Ganther R (2002) Reduction of CF<sub>4</sub> emissions from the aluminum smelter in Essen. In: Schneider W (ed) *Light Metals* 2002, pp. 297–304
- Wong DS, Fraser P, Lavoie P et al (2015) PFC emissions from detected versus nondetected anode effects in the aluminum industry. *JOM* 67:342–353. doi:10.1007/s11837-014-1265-8